Supporting Information

Preiss et al. 10.1073/pnas.1303333110

SI Materials and Methods

Cloning of Extended c-Ring Mutants and Construction of Mutants with a Five-Amino Acid Extended c-Subunit. The extended mutants of *Bacillus pseudofirmus* OF4 WT, A16G and A16/20G, were constructed as described previously (1, 2). In brief, 15 nucleic acid base pairs encoding five amino acids (alanine, asparagine, proline, phenylalanine, valine) were introduced into a *atpBEF* fragment in a low-copy plasmid (pMW118; Nippon Gene) using the GeneTailor Site-Directed Mutagenesis System (Invitrogen). The primers were F-ext5 5′-TCTCATTATTAATCTTATTCGCAAATCCTTTTGTTTAATCAGCAAT-3′ and R-ext5 5′-GAATAAGATTAATAATGAGATAACGATCGC-3′. The pMW118-Fo-Ext5 plasmids were used as a template to create the A16G and A16/20G mutations in the c-subunit, using the primers described by Liu et al. (1). The resulting plasmids were designated pMW118-Fo-A16G-Ext5 and pMW118-Fo-A16/20G-Ext5. The insertion fragments with correct mutations were released from pMW118 constructs and then reinserted into pG^+host4 (Appligene). The three recombinant constructs in pG^+host4 were transformed into a ΔF_o (Δ*atpB-F*) strain with a His-tagged β subunit (2). Following a two-step homologous recombination method, the mutants with the desired mutations were screened and confirmed by sequencing the entire *atp* operon, performed by Genewiz.

Growth Experiments in *B. pseudofirmus* OF4 WT and Mutant Cells. The growth curves (Fig. S5) were performed at either pH 7.5 [buffered with 100 mM 3-(*N*-morpholino)propanesulfonic acid (Mops)] or pH 10.5 (buffered with 100 mM sodium carbonate/bicarbonate), with either 50 mM glucose or 50 mM sodium malate as the carbon and energy source (3). The media also contained 0.1% yeast extract. Growth experiments were conducted in 96-well plates at 30 °C (4). Precultures were grown in glucose medium (pH 7.5) and diluted with Mops buffer (pH 7.5) to a final A_{600} of 0.005 without a washing step. The molar growth yields were determined as described previously (4), with minor modifications. Precultures were grown in glucose medium at pH 10.5, and a volume equivalent to 5 absorbance units (A_{600}) was subjected to a carbonate/bicarbonate buffer (pH 10.5) wash and then suspended in the same buffer at 5 A_{600} units/mL. Then 0.2 mL of the washed cell suspension was passed into 50 mL of pH 7.5 or pH 10.5 media (3) with 0.1% yeast extract, without or with 5 mM L-malate, at 37 °C. The maximum growth, measured as A_{600}, on yeast extract alone, which was determined to be fermentative because a ΔF_o mutant could grow on the yeast extract, was subtracted from the maximum growth on malate, and the dry weight was ascertained from a standard curve relating the A_{600} to the dry weight. The malate consumed at that time point was determined by assaying samples using an L-malate kit (Sigma-Aldrich).

Purification of *Geobacillus kaustophilus* c-Ring from Native Cells. *G. kaustophilus* (DSM 7263) was grown in LB medium at 55 °C for 22 h and harvested at 3,600 × *g* for 30 min at 4 °C. Then 30 g of cells (wet wt) were broken by four passages through a microfluidizer (Microfluidics). Unbroken cells and cell debris were removed by centrifugation at 14,000 × *g* for 20 min at 4 °C. Membranes were collected at 125,000 × *g* for 1 h at 4 °C and resuspended in 50 mM Tris·HCl (pH 8.0), 5 mM $MgCl_2$, 10% (vol/vol) glycerol, and 100 mM NaCl to a final concentration of 20 mg/mL For c-ring extraction, 1% *N*-lauroylsarcosine (Sigma-Aldrich) and 5 mM EDTA was added, and the sample was incubated for 10 min at 65 °C, followed by centrifugation at 125,000 × *g* for 1 h at 4 °C. The clarified supernatant was precipitated in 65% saturated $(NH_4)_2SO_4$ for 30 min at room temperature and then centrifuged at 8,500 × *g* for 20 min to pellet precipitated proteins. Then 0.05% n-dodecyl-ß-D-maltoside (DDM) was added to the resulting supernatant, followed by dialysis against 20 mM Tris·HCl (pH 8.0) overnight to remove the residual $(NH_4)_2SO_4$. Further purification was provided using Q-Sepharose anion exchange material (GE Healthcare).

The protein sample was bound to 10 mL of equilibrated [buffer A: 20 mM Tris·HCl (pH 8.0), 150 mM NaCl, and 0.05% DDM] column material, the column was washed with 5 column volumes (CV) of buffer A, and the protein was eluted using buffer A containing 0.8 M NaCl. The sample was desalted using a PD-10 column to 20 mM Tris·HCl (pH 8.0) and 0.05% DDM and applied to a MonoQ-Ion exchanger column (GE Healthcare), which was washed with 7.5 CV of buffer A, 7.5 CV of 10% buffer C [20 mM Tris·HCl (pH 8.0), 1 M NaCl, and 0.05% DDM]. The protein was eluted from the column in a continuous gradient from 10% to 100% buffer C in 10 CV. The c-ring–containing fractions were concentrated by ultrafiltration with a Sartorius Vivaspin concentrator (polyethersulfone membrane, 50K molecular weight cutoff; Fisher Scientific), and applied to a Superose 6 size-exclusion column (GE Healthcare) for final purification [20 mM Tris·HCl (pH 8.0) and 0.05% DDM].

Stability Test of WT and Mutant *B. pseudofirmus* OF4 c-Rings. For this test, 1 μg of WT and mutant (extWT, extA16G, and extA16/20G) c-ring samples were incubated with 100 mM malate/HCl (pH 2.0), 100 mM Tris·HCl (pH 8.0), or *N*-cyclohexyl-3-aminopropanesulfonic acid/NaOH (pH 11.5) at 20 °C or 85 °C for 30 min, and then analyzed by 13.2% SDS/PAGE as described previously (5). As a control, 1 μg of c-ring was monomerized by the addition of 15% (vol/vol) trichloroacetic acid (TCA) (6).

Atomic Force Microscopy. Contact-mode atomic force microscopy (AFM) was done with an atomic force microscope equipped with a 100-μm X-Y piezo scanner (Digital Instruments NanoScope IIIa; Veeco) and 200-μm 0.05 N/m cantilevers (OMCL RC-800-PS; Olympus). The c-ring samples were diluted to a final concentration of ∼10 μg/mL and adsorbed onto freshly cleaved mica in an adsorption buffer [300 mM KCl, 25 mM $MgCl_2$, and 20 mM Tris·HCl (pH 8.0)] for 15 min, then washed with an imaging buffer [150 mM KCl and 20 mM Tris·HCl (pH 8.0)]. The topographs were recorded at 25 °C at a maximal loading force of 100 pN and an optimized line scanning frequency of 5–7 Hz. Image processing was done using NanoScope (Veeco), BOXER (7), and IMAGIC (8). Diameters of the oligomers were measured at full-width half-protrusion from the lipid bilayer using NanoScope V software. Galleries of well-resolved particles were created using the BOXER manual particle picking procedure and further classified in IMAGIC. Results of the classification were further confirmed by eye in the unprocessed topographs, to assign c-rings to classes of each stoichiometry. To improve the quality of the averages, c-rings from series of topographs were pooled together to ensure more than 200 particle datasets for averaging for WT, more than 1,900 datasets for extWT, and more than 700 datasets for extA16G and extA16/20G. All molecules have the same in-plane orientation in the membrane of tightly packed vesicles, and averaging was performed by crystallographic methods with no reference bias. Counting of c-subunits in the c-rings was performed as described previously (9).

Data Collection, Structure Determination, and Refinement. Data to 4.1 Å were collected from a single crystal at the Max Planck/Novartis beamline X10SA (PX-II) of the Swiss Light Source, Villigen, Switzerland and processed using the XDS package (10). The phases were determined by molecular replacement (MR) using PHASER (11), with a search model of a c_{12} ring built from the c_{13} ring structure (PDB code 2x2v). In contrast to the $P2_1$ space group found for the WT c_{13} crystals (12), the A16/20G c_{12} ring formed crystals in space group $P2_12_12_1$ (Fig. S7). The MR trials performed with c_{12} and c_{13} unequivocally support the stoichiometry of 12 subunits in this c-ring (Fig. S8). Iterative cycles of model building and refinement were performed using COOT and phenix.refine of the PHENIX package, respectively. Noncrystallographic symmetry operation was applied during refinement. The model was energy-optimized during refinement by several cycles of simulated annealing. The refinement resulted in an electron density map in which the protein backbone was unambiguously traceable, including several individual side chains with 99.5% of the residues within the allowed regions of the Ramachandran plot. To further optimize and verify correct positioning of the side chains, Scwrl4.0 was used for side chain conformation prediction (13).

1. Liu J, Fujisawa M, Hicks DB, Krulwich TA (2009) Characterization of the functionally critical AXAXAXA and PXXEXXP motifs of the ATP synthase c-subunit from an alkaliphilic *Bacillus*. *J Biol Chem* 284(13):8714–8725.
2. Liu J, et al. (2011) Mutations in a helix-1 motif of the ATP synthase c-subunit of *Bacillus pseudofirmus* OF4 cause functional deficits and changes in the c-ring stability and mobility on sodium dodecyl sulfate-polyacrylamide gel electrophoresis. *Biochemistry* 50(24):5497–5506.
3. Wang Z, Hicks DB, Guffanti AA, Baldwin K, Krulwich TA (2004) Replacement of amino acid sequence features of *a*- and *c*-subunits of ATP synthases of alkaliphilic *Bacillus* with the *Bacillus* consensus sequence results in defective oxidative phosphorylation and non-fermentative growth at pH 10.5. *J Biol Chem* 279(25):26546–26554.
4. Liu J, Hicks DB, Krulwich TA (2013) Roles of AtpI and two YidC-type proteins from alkaliphilic *Bacillus pseudofirmus* OF4 in ATP synthase assembly and nonfermentative growth. *J Bacteriol* 195(2):220–230.
5. Schägger H, von Jagow G (1987) Tricine-sodium dodecyl sulfate-polyacrylamide gel electrophoresis for the separation of proteins in the range from 1 to 100 kDa. *Anal Biochem* 166(2):368–379.
6. Meier T, Ferguson SA, Cook GM, Dimroth P, Vonck J (2006) Structural investigations of the membrane-embedded rotor ring of the F-ATPase from *Clostridium paradoxum*. *J Bacteriol* 188(22):7759–7764.
7. Ludtke SJ, Baldwin PR, Chiu W (1999) EMAN: Semiautomated software for high-resolution single-particle reconstructions. *J Struct Biol* 128(1):82–97.
8. van Heel M, Harauz G, Orlova EV, Schmidt R, Schatz M (1996) A new generation of the IMAGIC image processing system. *J Struct Biol* 116(1):17–24.
9. Pogoryelov D, et al. (2012) Engineering rotor ring stoichiometries in the ATP synthase. *Proc Natl Acad Sci USA* 109(25):E1599–E1608.
10. Kabsch W (1993) Automatic processing of rotation diffraction data from crystals of initially unknown symmetry and cell constants. *J Appl Cryst* 26:795–800.
11. McCoy AJ (2007) Solving structures of protein complexes by molecular replacement with Phaser. *Acta Crystallogr D Biol Crystallogr* 63(Pt 1):32–41.
12. Preiss L, Yildiz Ö, Hicks DB, Krulwich TA, Meier T (2010) A new type of proton coordination in an F_1F_o-ATP synthase rotor ring. *PLoS Biol* 8:e000443.
13. Krivov GG, Shapovalov MV, Dunbrack RL, Jr. (2009) Improved prediction of protein side-chain conformations with SCWRL4. *Proteins* 77(4):778–795.
14. Stahlberg H, et al. (2001) Bacterial $Na^{(+)}$-ATP synthase has an undecameric rotor. *EMBO Rep* 2(3):229–233.
15. Vonck J, et al. (2002) Molecular architecture of the undecameric rotor of a bacterial Na^+-ATP synthase. *J Mol Biol* 321(2):307–316.
16. Matthies D, et al. (2009) The c_{13} ring from a thermoalkaliphilic ATP synthase reveals an extended diameter due to a special structural region. *J Mol Biol* 388(3):611–618.
17. Meier T, Matthey U, Henzen F, Dimroth P, Müller DJ (2001) The central plug in the reconstituted undecameric c cylinder of a bacterial ATP synthase consists of phospholipids. *FEBS Lett* 505(3):353–356.
18. Pogoryelov D, et al. (2007) The oligomeric state of c rings from cyanobacterial F-ATP synthases varies from 13 to 15. *J Bacteriol* 189(16):5895–5902.

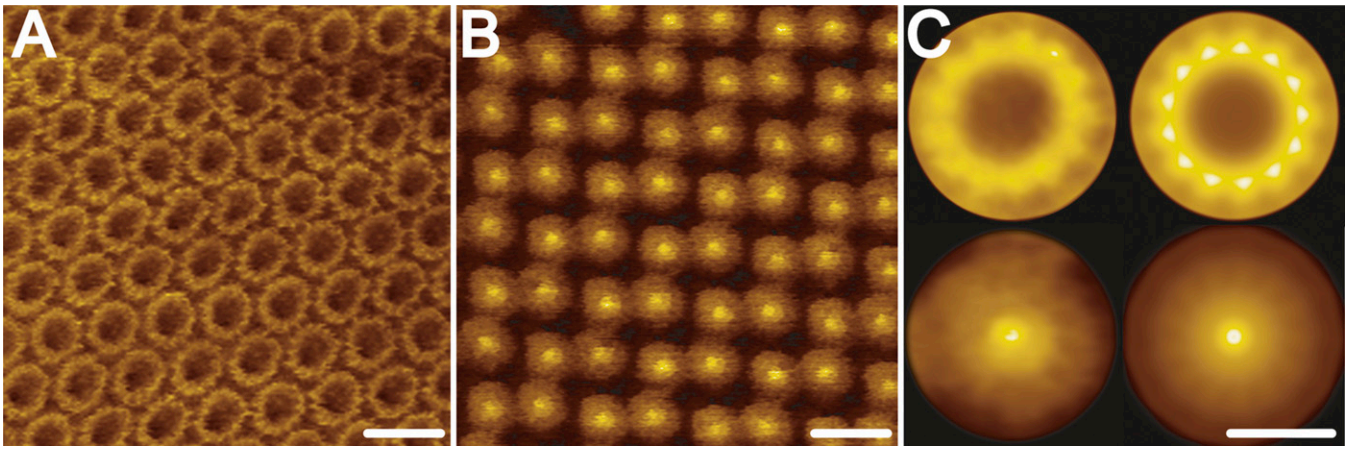

Fig. S1. AFM topographs of reconstituted *B. pseudofirmus* OF4 c-rings. (Nonextended) WT *B. pseudofirmus* OF4 c_{13} rings were purified and densely reconstituted in lipid vesicles. Small, quasi- 2D crystalline lattices were obtained and analyzed by high-resolution AFM. The topographs show c-rings packed in two different orientations, viewed from their cytoplasmic (*A*) and periplasmic (*B*) sides (14–16), without and with a central mass, respectively. The central mass is formed by a bundle of lipids (17). The quality of the AFM topographs allowed analysis of the cytoplasmic side of the c-rings, but was not sufficiently high to unambiguously determine the stoichiometry of the rings viewed form the periplasmic side in unprocessed images. (*C*) Processed images. Nonsymmetrized (*Left*) and symmetrized (*Right*) reference-free single-particle averages of the cytoplasmic side (*Upper*; $n = 50$) and the periplasmic side (*Lower*; $n = 50$), both confirming the 13-fold c-ring stoichiometry, as reported previously (12). (Scale bars: 10 nm in *A* and *B*; 5 nm in *C*.)

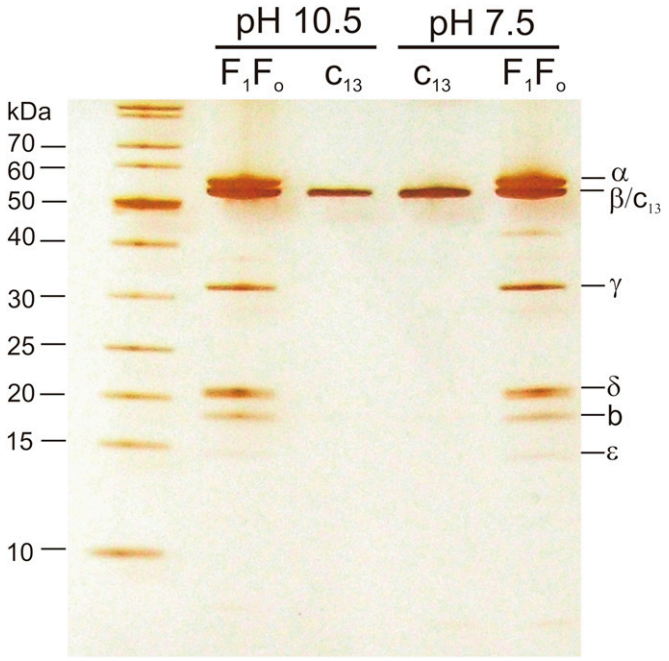

Fig. S2. Comparison of purified F_1F_o-ATP synthase and c-rings from cells grown at pH 10.5 and pH 7.5. *B. pseudofirmus* OF4 cells were grown at pH 10.5 and 7.5. The ATP synthase and their (nonextended) c-rings were purified and compared on a 13.2% SDS-polyacrylamide gel. The enzymes show identical migration patterns for all subunits (indicated on the right). The c-rings isolated from these two ATP synthase fractions show the same migration level, with a c-ring stoichiometry of 13 in both cases. Thus, the pH of the growth medium has no influence on the stoichiometry of the *B. pseudofirmus* OF4 c-ring.

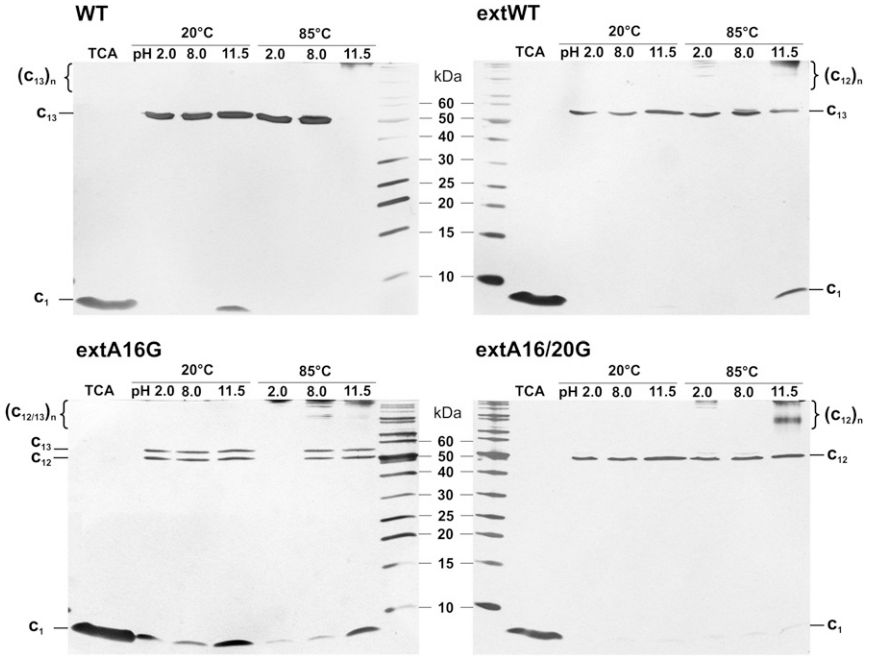

Fig. S3. Temperature and pH stability of (nonextended) WT, extWT, and extended mutant c-rings. The *B. pseudofirmus* OF4 c_{13} oligomer exhibits remarkably high resistance to detergents like SDS, as well as to environmental pH and temperature. Neither pH nor temperature in the tested range disassembled the oligomeric complex. High and low pH values in combination with high temperature led to aggregation of the ring rather than monomerization. To ensure that this property remained unchanged in the mutants, and that the observed changes in stoichiometry were not purification artifacts caused by reduced complex stability, we compared pH and temperature stability of purified mutant c-rings with WT c-rings. All WT and mutant c-rings were incubated at temperatures up to 85 °C in DDM-containing buffers with pH varying from 2.0 to 11.5, after which the material was analyzed by SDS/PAGE. In all cases, acidification with TCA was performed to disintegrate the protein complexes to c-monomers. The extA16G mutant demonstrated slightly reduced resistance toward acidic treatment, whereas the WT, extWT, and extA16/20G double mutant showed no significant difference in stability of the oligomeric assembly. Thus, the resistance to heat and pH of all extended mutants, including the c_{12} ring, is similar to that of the WT c_{13} ring, indicating that the new c-ring stoichiometry is an energetically favorable conformation that can be induced by only one or two mutations.

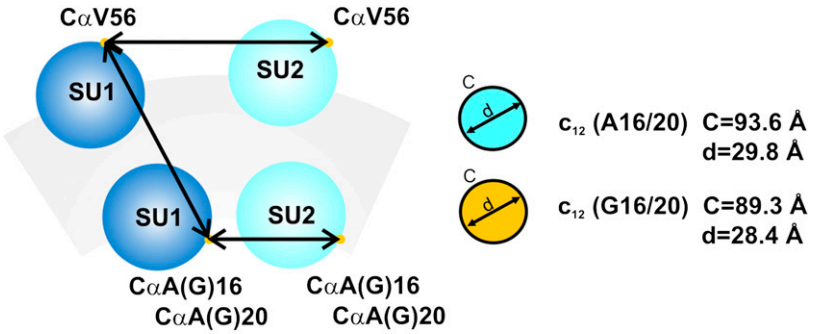

average residue distances (Cα) (Å)	c_{13} (WT) measured	c_{12} (WT) calculated	c_{12} (G16/20) measured
16-16 - inner helices	7.81		7,44
20-20 - inner helices	8.38		8.09
16-56 - intra c-subunit	8.93 (±0.07)		8.68 (±0.29)
56-56 - outer helices	11.24		11.15
circumference (C) on A16/G16 level	101.53	93.6	89.3
circumference (C) on A20/G20 level	108.94	100.56	97.08

Fig. S4. Helix-helix packing and distances in the A16/20G c_{12} mutant ring. Distances of Cα atoms of subunit 1 (SU1; dark blue) to Cα atoms of subunit 2 (SU2; light blue) were measured to compare the packing of the helices in the c_{12} and c_{13} WT c-rings. Whereas the distance of Val56 Cα in SU1 to Ala16 Cα in SU1 changed to an insignificant degree, the distance of Ala16 Cα (SU1) to Ala16 Cα (SU2) was significantly shorter, as was the distance of Ala20Cα (SU1) to Ala20Cα (SU2). This reduced the c-ring circumference of the A16/20G mutant compared with a theoretically calculated c_{12} circumference with the WT sequence by 3.5 Å on the G16 level or by 4 Å on the G20 level (*Results*).

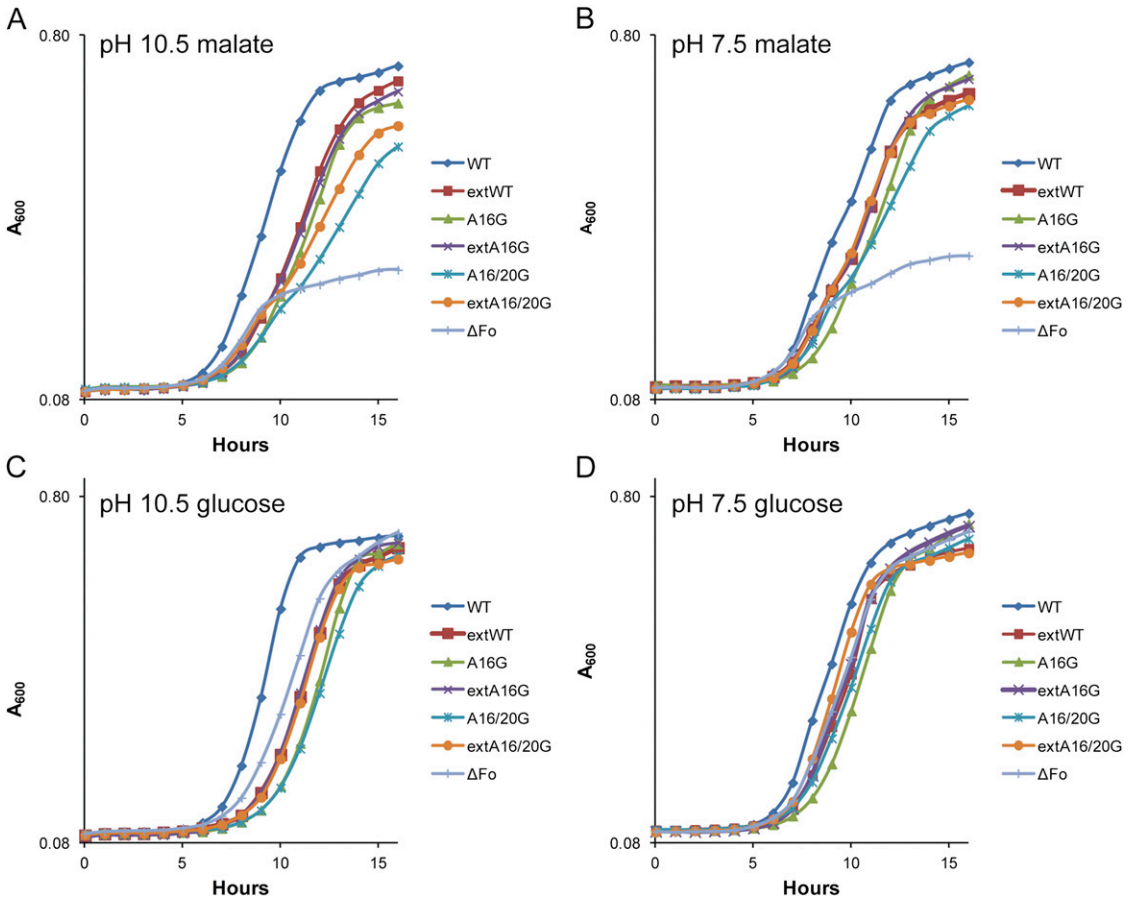

Fig. S5. Growth curves of strains harboring ATP synthases with extended or nonextended c-rings. The growth curves were determined at 30 °C as described in *Materials and Methods*. The curves represent the averages of three independent growth curves, each done in duplicate. (*A*) pH 10.5 malate. (*B*) pH 7.5 malate. (*C*) pH 10.5 glucose. (*D*) pH 7.5 glucose.

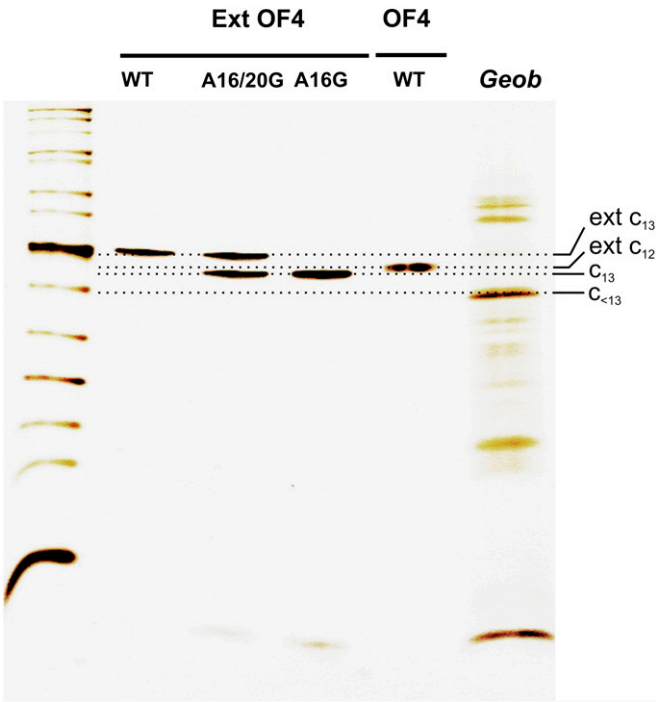

Fig. S6. Comparison of *B. pseudofirmus* OF4 WT and mutant c-rings with C-terminal extension and c-ring from the neutralophile *G. kaustophilus*. The mobility of oligomeric c-rings on SDS/PAGE is proportional to their molecular weight and hence to their stoichiometry (18). The c-ring isolated from the neutralophilic *G. kaustophilus* migrates faster than the c-rings from *B. pseudofirmus* OF4 with known stoichiometries of c_{12} and c_{13}, but has a similar c-subunit molecular mass (*B. pseudofirmus* OF4, 6,956 Da; *G. kaustophilus*, 7,333 Da). Thus, the c-ring from the neutralophile has a smaller stoichiometry ($c_{<13}$) than the c-rings from the alkaliphile.

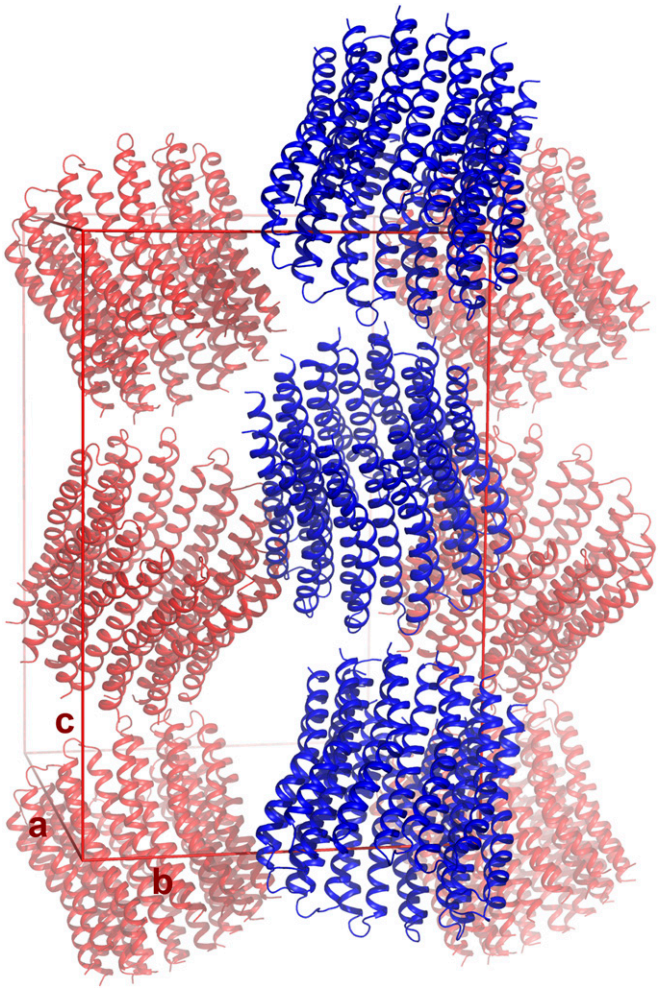

Fig. S7. Crystal packing of the *B. pseudofirmus* OF4 A16/20G c_{12} ring. The c_{12} ring was crystallized in 3D without extension in the space group $P2_12_12_1$. Each ring contacts three other rings with its loop region and one other ring with its C-termini. Although the extension improved the protein packing in two dimensions, it turned out to have a negative effect on packing in three dimensions, possibly owing to the crystal contact at the N terminus, which might be prevented by extending the C-terminus in this c-ring.

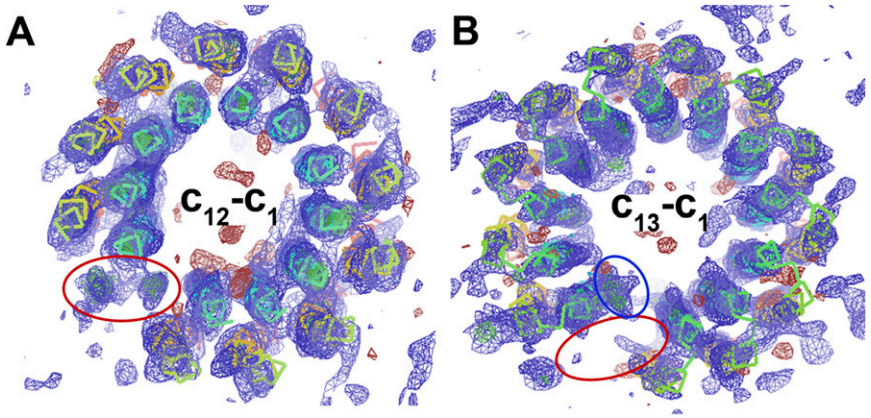

Fig. S8. Molecular replacement using *B. pseudofirmus* OF4 c_{12} and c_{13} ring models. MR with PHASER was performed using c_{12} minus $1c_1$ ($c_{12} - c_1$) and c_{13} minus $1c_1$ ($c_{13} - c_1$) models to verify the changed stoichiometry from c_{13} to c_{12} in the A16/20G mutant. (*A*) A c_{12} ring with one subunit deleted ($c_{12} - c_1$) was used as an initial model for MR. The obtained solution showed a high translation factor *z*-score (TFZ) of 11.3 and a log-likelihood gain (LLG) of 381, with densities that covered the complete α-helices of the model. Moreover, a density for the missing subunit appeared and completed the c_{12} ring (red circle), which is a strong indication that the chosen stoichiometry of 12 is correct. (*B*) The MR result obtained with the $c_{13} - c_1$ model yielded a TFZ of only 8.5, and the resulting densities appeared less clear. In addition, there was no density visible for the deleted subunit (red circle), but a density appeared suggesting a smaller ring diameter than in the model (blue circle).

Table S1. Data collection and refinement statistics, A16/20G crystal

Parameter	Value
Data collection	
Space group	$P2_12_12_1$
Cell dimensions	
a, *b*, *c*, Å	90.4, 114.3, 137.6
α, β, γ, °	90, 90, 90
Resolution, Å	44.95–4 (4.35–4.1)
R_{meas}	15.5 (97.8)
$R_{mergd\text{-}F}$	39.9 (126.7)
I/σI	7.29 (1.85)
Completeness, %	98.7 (93.9)
Redundancy	3.57
Refinement	
Resolution, Å	48.9–4.1
Number of reflections	11,501
R_{work}/R_{free}, %	27.5/33.5
Number of atoms	
Protein	5,822
B-factors	
Protein	45.6
rms deviations	
Bond length, Å	0.005
Bond angle, °	1.13

Numbers in parentheses refer to the highest-resolution shell.